Rep Pract Oncol Radiother, 2006; 11(3): 123-133

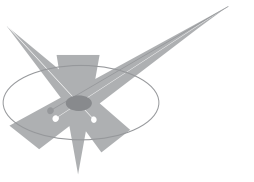

Original Paper

**Received:** 2005.10.11
**Accepted:** 2006.04.05
**Published:** 2006.06.28

# Experimental and Monte Carlo evaluation of Eclipse treatment planning system for lung dose calculations

**Asghar Mesbahi**[1 ABCDEF], **David I. Thwaites**[2 BCDG], **Andrew J. Reilly**[2 CDG]

[1] Medical Physics Department, Medical School, Tabriz University of Medical Sciences, Tabriz, Iran
[2] Oncology Physics Department, Western General Hospital, Edinburgh, U.K.

**Authors' Contribution:**
A Study Design
B Data Collection
C Statistical Analysis
D Data Interpretation
E Manuscript Preparation
F Literature Search
G Funds Collection

## Summary

**Background** In this study the accuracy of a pencil beam based treatment planning system (TPS) was evaluated for lung dose calculations by comparison with measurement and the Monte Carlo (MC) method.

**Aim** In the current study we assessed the performance of the Eclipse treatment planning system in the thorax region by ionization chamber measurements and Monte Carlo calculations. We examined two analytic methods: modified Batho (MB) and equivalent tissue-air ratio "ETAR" methods for thorax region irradiations. For Monte Carlo calculations in the thorax phantom, we modelled a Varian Clinac 2100EX linac. After benchmarking our model with water phantom measurements we used this model for thorax phantom calculations.

**Materials/Methods** 8 and 15MV photon beams of Varian 21EX linac were used for irradiations. Using MANP4C Monte Carlo code, the geometry of the linac head was simulated. After commissioning "MC" beam models, lung doses were calculated by the Monte Carlo (MC) method. Irradiation cases were: (1) posterior fields of single lung with field sizes of 4×4 and 10×10cm$^2$ (2) lateral fields of thorax with 4×4 and 10×10cm$^2$ field sizes.

**Results** TPS calculations involving ETAR and MB methods were in close agreement with Monte Carlo results and measurements for a 10×10 cm$^2$ field size at both energies. For a field size of 4×4cm$^2$ the maximum differences in local dose between TPS calculations and measurement were +33% (MB) and +28% (ETAR). Also, they ignored lung dose reduction due to lateral electronic equilibrium for small field size. Similar results would be expected for other TPSs implementing these algorithms. MC calculations were in excellent agreement with measurement, showing local differences of no more than 2% for all measured points.

**Conclusions** Our study findings showed great differences between both analytical methods and measurements for 4×4cm$^2$ field sizes for points in the lung. Our study recommends using the MC method for small-field lung dose calculations.

**Key words** **radiotherapy treatment planning • Monte Carlo method • lung inhomogeneity • thorax phantom • electronic equilibrium**

**Full-text PDF:** http:/www.rpor.pl/pdf.php?MAN=9161

**Word count:** 3380
**Tables:** 2
**Figures:** 8
**References:** 30

**Author's address:** Asghar Mesbahi, Medical Physics Department, Medical School, Tabriz University of Medical Sciences, Tabriz, Iran, e-mail: asgharmesbahi@yahoo.com

## Background

For the important step of dose calculation in treatment planning, the necessary accuracy may be required to be within 2–3%, so that an overall accuracy of 5% can be attained [1,2]. To achieve such high accuracy in dose calculation requires both detailed and accurate anatomical information, and rather rigorous and accurate dose calculation algorithms. The most common analytic methods for inhomogeneity correction are effective path length (EPL), Batho, equivalent tissue-air ratio (ETAR) and differential scatter-air ratio (DSAR) methods. One of the basic limitations of all these methods is that they can only account for the transport of photons, while the loss of electron equilibrium near interfaces and within heterogeneous media is ignored [3–13]. In order to assess the accuracy of dose calculation algorithms used in treatment planning, therefore, a rigorous dose calculation method in inhomogeneous media is desired. The Monte Carlo method is the most complete and accurate dose calculation method, since it can accurately account for density and atomic number variations within the patient by simulating photon and electron transport and scoring energy deposition. MCNP Monte Carlo code has been benchmarked with experimental data by many investigators and used for Monte Carlo dose calculations in radiotherapy [14,15].

There are many papers in the literature about inhomogeneity correction and Monte Carlo methods for lung dose calculations [14,16–22]. But in most of them there is not a sufficiently reliable practical dosimetry system for comparisons and they lack quantitative results for comparison with calculation methods [18]. On the other hand, although the results of previous studies about inhomogeneity correction methods have shown that analytic methods such as EPL, Batho, ETAR, and DSAR are not able to provide accurate results for the lung region, due to the simplicity of computerized implementations and calculation speed they are used in current treatment planning systems [14]. However, knowledge about the advantages and deficiencies of commercial treatment planning systems used for conventional or conformal radiotherapy remains an important responsibility for medical physicists in radiotherapy departments.

## Aim

In the current study we assessed the performance of the Eclipse treatment planning system in the thorax region by ionization chamber measurements and Monte Carlo calculations. We examined two analytic methods: modified Batho (MB) and equivalent tissue-air ratio "ETAR" methods for thorax region irradiations. For Monte Carlo calculations in the thorax phantom, we modelled a Varian Clinac 2100EX linac. After benchmarking our model with water phantom measurements we used this model for thorax phantom calculations.

## Materials and Methods

### Monte Carlo simulations

We developed a photon beam model for the Varian 2100EX linac for dose calculation purposes using MCNP4C Monte Carlo code. We used 8 and 15MV photon beams for our study.

A schematic representation of the linac head and its components is shown in Figure 1. The linac head components including target, primary collimator, flattening filter and secondary collimator jaws were simulated based on manufacturer provided information. No energy spread for the electron beam was considered because this parameter has shown no considerable influence on beam profile or depth dose curves [23,24]. A mono-energetic electron beam with uniform spatial distribution and 2 mm diameter was considered for the electron beam. The electron beam width of 2 mm for both beams was assumed a default value [25].

First, electron beam energy selection was performed by comparing measured and calculated

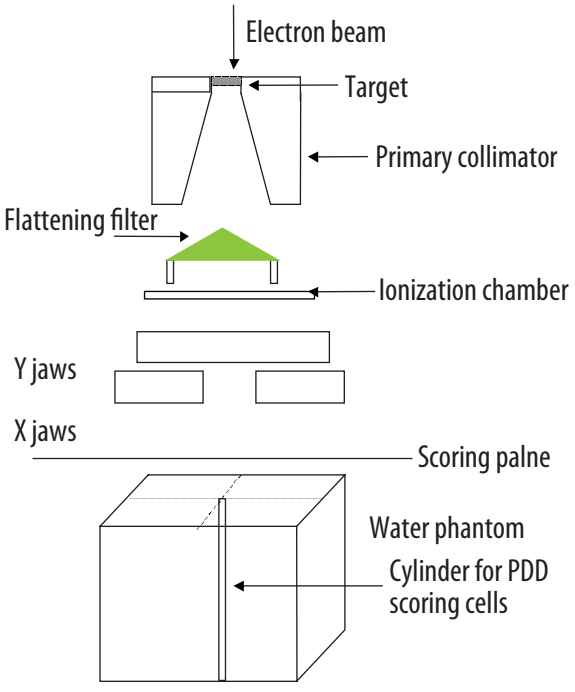


**Figure 1.** Schematic representation of Varian Clinac 2100EX and simulated geometry including position of scoring plane for phase space file generation and water phantom.

percentage depth dose (PDD) curves. Then, PDD curves and beam profiles of both photon beams for 4×4, 10×10 and 20×20cm$^2$ field sizes were calculated and compared with measured data. The beam profiles were calculated in two depths of $d_{max}$ and 10cm. For each point the local difference relative to the measured dose at that point was calculated.

We performed the simulation process in two distinct steps. First, an initial Monte Carlo simulation of the accelerator head was performed to produce the phase space (PS) file for different field sizes and energies of the primary electron beam. Then we commissioned the beam model by assessing the percentage depth dose curves and beam profiles calculated in a water phantom and comparing with measured data.

A scoring plane for phase space file generation at 80cm distance from the target and 20cm above the water phantom was defined (Figure 1).

For dose calculations in the water phantom PS files were generated using from $15\times10^6$ to $5\times10^6$ initial electrons for 4×4 to 20×20cm$^2$, respectively. By running $15\times10^6$ electrons, $6\times10^6$ particles crossed the scoring plane and their history were recorded in the PS file. The size of the PS file varied from 2 to 3 GBytes depending on field size. Statistical uncertainty of MC results was less than 0.5% at $d_{max}$.

For optimum phase space generation, photon and electron energy cut-offs of 10 and 500KeV were used.

A water phantom with dimensions of 30×30×30cm$^3$ was simulated. A cylinder with radius equal to one-tenth of the beam diameter along the central axis of the beam was considered and divided into scoring cells with a height of 2mm. By running particles in the PS file through the water phantom, the energy deposited in each scoring cell was calculated by *F8 tally. For beam profile the same approach was used except that the central axis of the scoring cylinder was perpendicular to the central axis of the beam and two cylinders at two depths, $d_{max}$ and 10cm, were defined. The diameter of the cylinders was 4mm, divided into cells with 2mm thickness. The dose resolution for beam profiles was 2mm laterally.

For phase space file generation, the average run time for 10×10cm$^2$ field size was about 10 hours with a cluster composed of 13×2.6GHz Athelon processors. Tuning of electron beam energy was performed by comparing calculated and measured PDD for 10×10cm$^2$ field size. For the purpose of comparison between calculation and measurements, the value of each cell normalized to the maximum value of energy deposited in the central axis. To prevent the effect of noise on our normalization point, the average value of 3 maximum points was considered as a normalization value. The first run was started by the nominal energy of the photon beam and then the energy increased or decreased according to the result of the first comparison between calculations and measurements. For the 8MV photon beam energies of 8.0, 8.2, 8.3, 8.4 and 8.5, and for the 15MV photon beam energies of 15.0, 15.2, 15.3 and 15.4, were used. For primary electron energy determination the results of measurements and calculations were compared and the best match determined the optimum energy of the electron beam. Local differences between calculations and measurement results were calculated for accurate comparison between results. No polynomial fitting was used for MC calculated PDD curves and beam profiles.

**Thorax phantom**

We used an anatomic thorax phantom for our study. This phantom is shown in Figure 2. We used

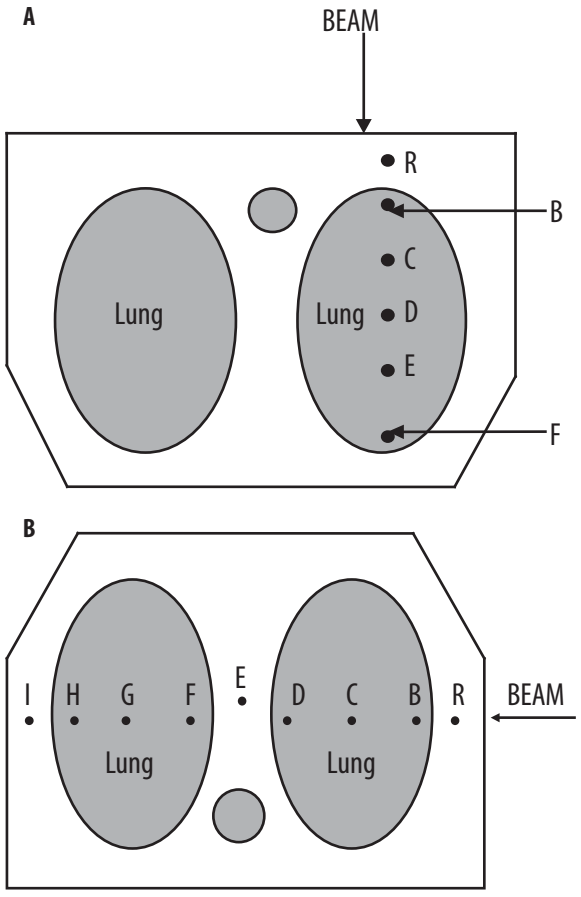


**Figure 2.** Schematic diagram of thorax phantom, illustrating (**A**) posterior and (**B**) lateral beam geometries.

ICRU report No. 48 to determine the dimensions of the phantom, based on the average thorax of an Asian male, including the dimensions of the lung and the thickness of the chest wall.

We modelled the thoracic spine using a Teflon (density=2g/cm$^3$) cylinder 20 cm in length and 3cm in diameter. Cork with a density of 0.2g/cm$^3$ was used for lung tissue. The phantom was constructed from polyethylene in place of soft tissue. For point dose measurements with an ionization chamber, several holes were made in polyethylene and cork. These holes were filled completely with the same size cylinders. One cylinder was drilled according to the external shape and size of the chamber. For dose measurement at a given point, the simple cylinder was replaced by this chamber fitted cylinder.

The mass densities of the polyethylene, Teflon and cork were determined by dividing the measured weight by the calculated volume, and were 0.94, 2.0 and 0.2g/cm$^3$ respectively.

**Dose measurements**

Dose measurements were taken using a scanditronix automatic blue phantom and ionization chamber with 0.125cc volume. The measurements were performed with 1mm resolution for both PDD curves and beam profiles. For comparison between measurement and calculations and better illustration, the results were reduced to 4mm resolution. Measured results were corrected for measurement point displacement of 1mm toward the phantom surface.

We assign an overall experimental accuracy of 0.5% in relative dose measurements with automatic water phantom. This uncertainty includes positioning inaccuracy of chamber up to 1mm and short-term fluctuations of chamber, electrometer, air pressure and temperature during the time frame of one scan.

Dose measurements in the thorax phantom were performed for both energies of 8 and 15MV beams with posterior and lateral fields. For point dose measurements in the phantom we used the Pinpoint chamber type 31006 with 0.015cm$^3$ sensitive volume and Unidose E-electrometer produced by PTW-Freiburgh. Three readings were recorded for each point of measurement and averaged and also corrected for temperature and pressure variations during the measurement. The reference point was in $d_{max}$ and all readings were normalized to $d_{max}$ reading. Experiment setup and measurement points are shown in Figures 1 and 2.

**Treatment planning system**

We used the Eclipse treatment planning system Rel.6.5 for our dose calculations. This system is part of the integrated imaging and 3D-dose calculation system from Varian medical systems. This system is a modified version of the Cadplan treatment planning system. This TPS can be used for open and MLC-shaped fields in 3D-conformal radiotherapy. All required data including the anatomic geometry of patient and electron densities of body tissues are derived from CT images. Dose calculations are performed based on a reconstructed 3D image of the patient. It utilizes a single pencil beam model in conjunction with one of three inhomogeneity correction methods: Batho power law, MB and ETAR. Simply, the dose value calculated in a water-equivalent material is multiplied by inhomogeneity correction factors calculated by these methods.

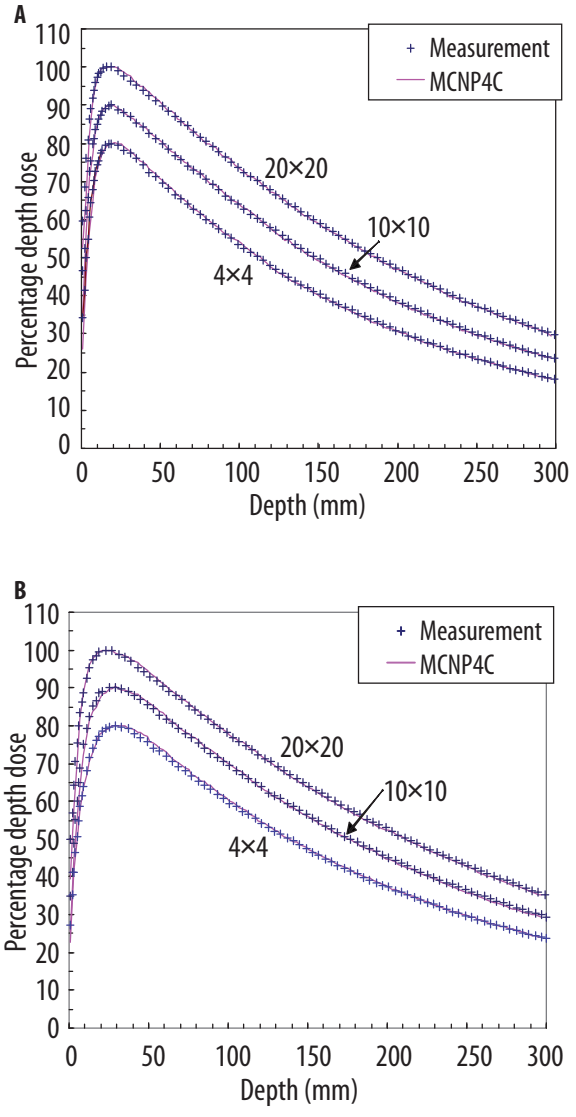


**Figure 3.** Comparison of calculated and measured percentage depth dose curves for (**A**) 8MV and (**B**) 15MV beams. The curves for 10×10 and 4×4cm$^2$ field sizes were scaled by 0.9 and 0.8 respectively for inclusion on the same graph.

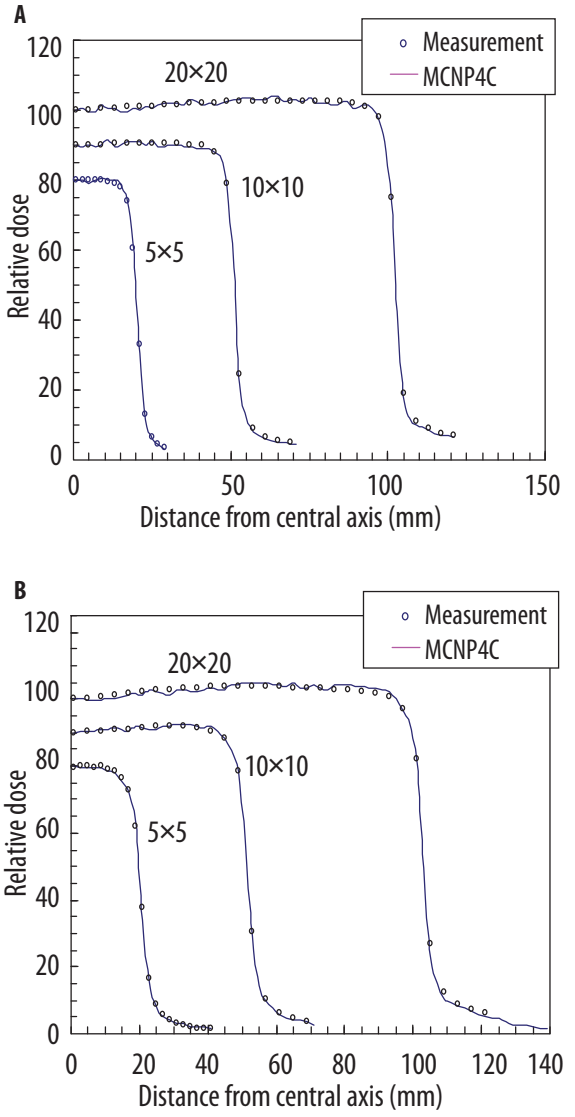


**Figure 4.** Comparison of calculated and measured beam profiles at $d_{max}$ for (**A**) 8MV and (**B**) 15MV photon beams.

The thorax phantom was scanned with 1mm slice thickness and its images transferred into the Eclipse system. Then the central axis dose distribution for field sizes of 4×4 and 10×10cm$^2$ and for posterior and lateral cases using 8 and 15MV photon beams was calculated. The results of calculations for all cases were transformed into text file for further quantitative analysis. Dose resolution of calculated central axis doses was 0.25mm.

### Irradiation geometries

Irradiation geometries are shown in Figure 2. It consists of: (1) posterior fields of single lung with field sizes of 4×4 and 10×10cm$^2$, (2) lateral fields of thorax with 4×4 and 10×10 cm$^2$ field sizes. Both cases were irradiated by 8 and 15MV beams.

## Results and Discussion

### Commissioning Monte Carlo model

By running the phase space file for depth dose calculation, the statistical uncertainty of the results was about 0.5% at $d_{max}$ for our PDD calculations in the water phantom. Comparing the calculated and measured PDD curves for 10×10 cm$^2$ field size, the mean energy of the electron beam for 8MV and 15MV photons was determined as 8.4±0.1 and 15.2±0.1 MeV, respectively. The local

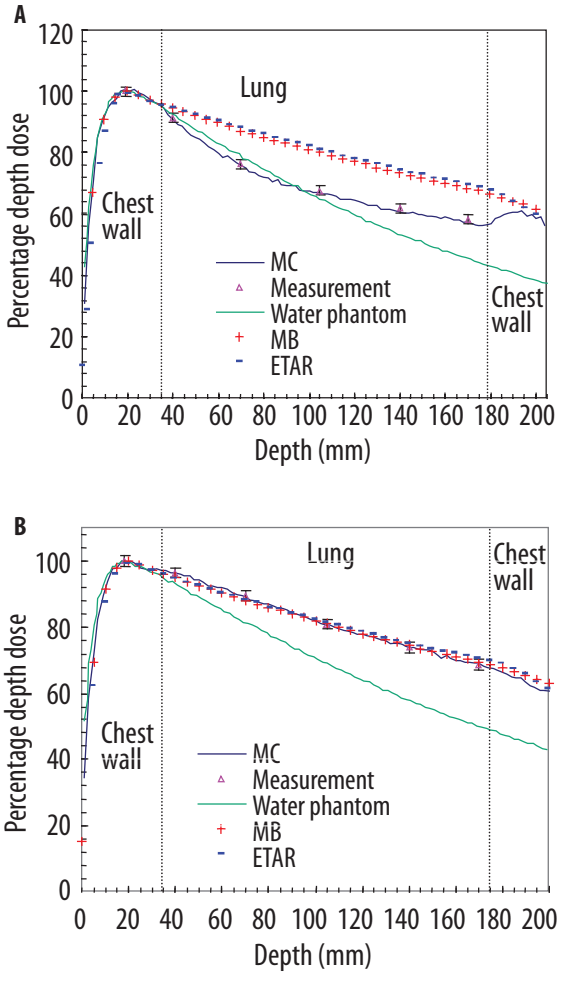


**Figure 5.** Comparison of percentage depth doses calculated by MB, ETAR and Monte Carlo methods and measurements for posterior lung irradiations by 8MV photon beam. (**A**) Field size=4×4cm$^2$, (**B**) Field size=10×10cm$^2$.

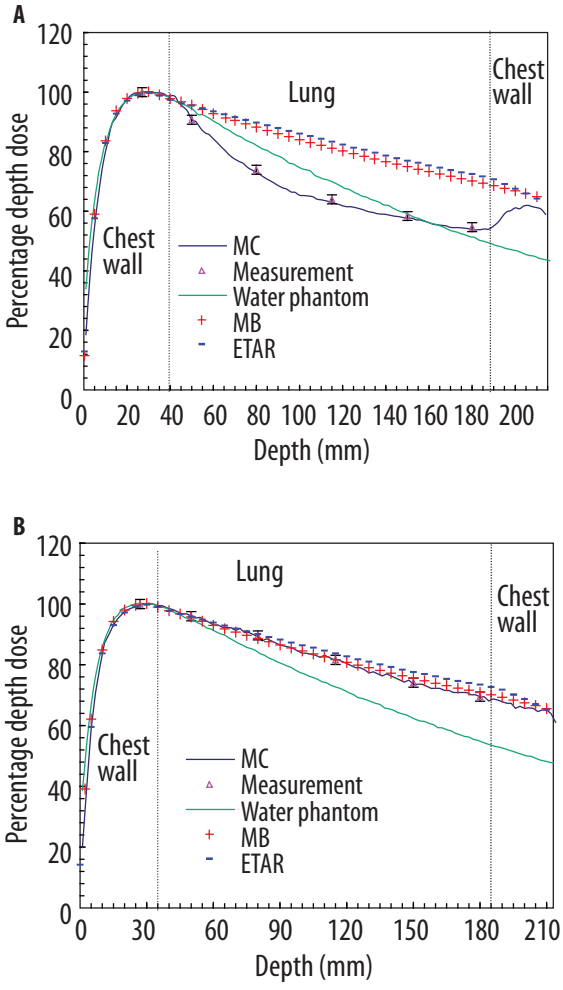


**Figure 6.** Comparison of percentage depth doses calculated by MB, ETAR and Monte Carlo methods and measurements for posterior lung field irradiations by 15MV photon beam. (**A**) Field size=4×4cm$^2$, (**B**) Field size=10×10cm$^2$.

differences between measurements and calculations are less than ±1.5% for the descending part of curves. We also calculated PDD curves for 4×4, 10×10 and 20×20cm$^2$ field sizes and compared with measurements. Comparisons between calculated and measured PDD curves for 8 and 15MV photon beams are shown in Figure 3. Statistical uncertainty less than 0.5% in $d_{max}$ allowed us to normalize the absorbed dose values to the depth of maximum dose for all PDD curves.

Our results were in accordance with those of Sheikh-Bagheri et al., which showed 1.5% local difference between calculated and measured results [23]. It was also less than the recommended value of 2% [26]. For the build-up region local differences up to 10% were seen. This difference was seen and reported in other studies [14,15,25]. It is due to the high gradient of dose distribution in that region, which makes ionization chamber measurements unreliable. Also, the finite size of the ionization chamber, which perturbs the absorbed dose, may be another reason for this large local difference [23–25].

Beam profiles for both energies were calculated at two depths, $d_{max}$ and 10cm. We also compared calculation results with measurements to validate our model. Comparisons for beam profiles at $d_{max}$ are shown in Figure 4. The statistical uncertainty of calculated beam profiles was between 0.6% and 1.3% in the flat region of profiles. For better comparison between measurement and calculations, we considered three regions in our profiles including: (1) flat or umbra region, (2) penumbra region, (3) low dose, out-of-field region [26].

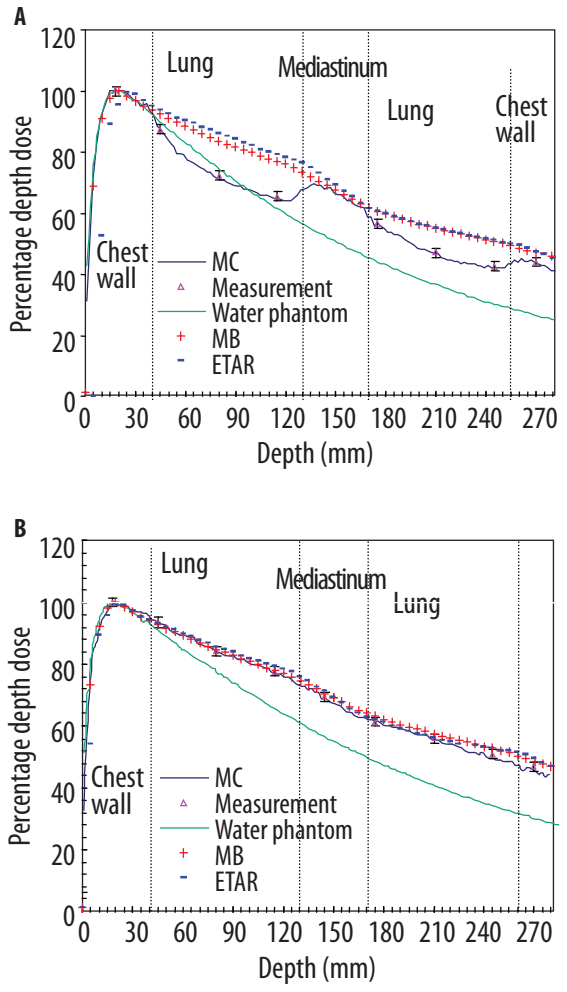


**Figure 7.** Comparison of percentage depth doses calculated by MB, ETAR and Monte Carlo methods and measurements for lateral thorax irradiations by 8MV photon beam. (**A**) Field size=4×4cm$^2$, (**B**) Field size=10×10cm$^2$.

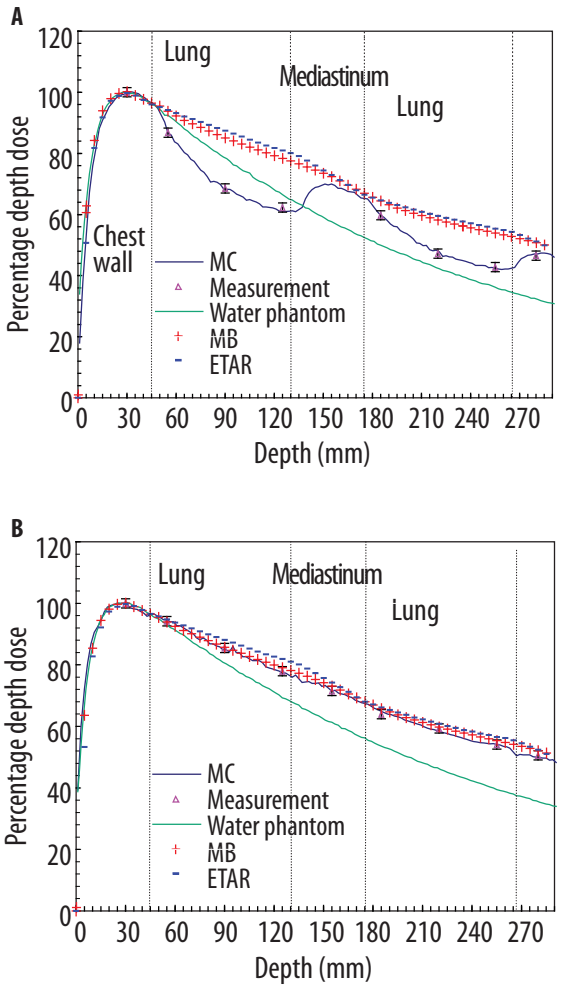


**Figure 8.** Comparison of percentage depth doses calculated by MB, ETAR and Monte Carlo methods and measurements for lateral thorax irradiations by 15MV photon beam. (**A**) Field size=4×4cm$^2$, (**B**) Field size=10×10cm$^2$.

For the flat region the local differences were up to 2% for all field sizes and depths. For the second region, local differences up to 10% were seen. In the low dose region, which is located outside the geometric border of the field, local differences were up 18%.

Comparing local differences found in our results with published criteria showed that our MC model results were acceptable and our model could be used for dose calculation in other situations and geometries [26].

### Comparisons for thorax field irradiations

The results of calculations by MB and ETAR and MC compared with measurements are shown for both energies and for both field sizes in Figures 5–8. We included depth dose curves of homogeneous water phantom in all graphs for comparison purposes. For quantitative evaluation of calculation methods, local differences between all methods and measurements are shown in Tables 1 and 2 for posterior or single lung and lateral cases, respectively.

As the figures show, for 10×10cm$^2$ field sizes there is good agreement between all calculation methods and measurement, with MB calculations agreeing slightly better than ETAR. The maximum differences in local dose for posterior irradiation geometry occurred for the 15MV beam and were +2.0% (MB) and +5.6% (ETAR). Similar results were observed for lateral irradiation geometry, with the maximum local differences also occurring at 15MV and being +4.4% (MB) and +5.6% (ETAR).

**Table 1.** Local differences of Modified Batho, Equivalent TAR and Monte Carlo calculations in comparison with measurement in posterior field irradiations for 8 and 15MV photon beams.

| Field size\Points | | B | C | D | E | F |
|---|---|---|---|---|---|---|
| 10×10cm$^2$ (8MV) | MC | −0.27 | −0.59 | −0.51 | +0.22 | +0.57 |
| | MB | +0.78 | +0.85 | +0.27 | +0.55 | +0.86 |
| | ETAR | −1.8 | −1.27 | +3.16 | +1.75 | +3.2 |
| 4×4cm$^2$ (8MV) | MC | −0.05 | −0.26 | −1.1 | −1.76 | −1.76 |
| | MB | +3.7 | +14.15 | +18.5 | +18.88 | +17.6 |
| | ETAR | +3.52 | +15.63 | +20.1 | +20.19 | +19.86 |
| 10×10cm$^2$ (15MV) | MC | +0.06 | −0.47 | +0.11 | −0.77 | −0.08 |
| | MB | −0.28 | −1.17 | +0.06 | +1.98 | +1.91 |
| | ETAR | −0.2 | +0.46 | +2.5 | +4.66 | +5.6 |
| 4×4cm$^2$ (15MV) | MC | +0.16 | −1.05 | −1.68 | −1.29 | −1.5 |
| | MB | +5.53 | +19.32 | +26.83 | +28.35 | 28.39 |
| | EATR | +5.23 | +21.45 | +30.23 | +31.7 | +32.64 |

**Table 2.** Local differences of Modified Batho, Equivalent TAR and MCNP4C calculations in comparison with measurement in lateral field irradiations for 8 and 15MV photon beams.

| Field size\Points | | B | C | D | E | F | G | H | I |
|---|---|---|---|---|---|---|---|---|---|
| 10×10cm$^2$ (8MV) | MC | +0.19 | +0.1 | −0.57 | −1.1 | +0.43 | −0.6 | −2 | −1.9 |
| | MB | −0.6 | +0.66 | +0.24 | +1.53 | +2.86 | +2.35 | +3.52 | +4.41 |
| | ETAR | −0.46 | +1.84 | +1.97 | +2.28 | +0.82 | +0.19 | +2.5 | +3.56 |
| 4×4cm$^2$ (8MV) | MC | +0.27 | −1.42 | −1.09 | – | +0.27 | +1.54 | −1.84 | −0.62 |
| | MB | +5.8 | +15.47 | +17.58 | – | +7.43 | +16.81 | +21.6 | +6.30 |
| | ETAR | +5.8 | +17.78 | +19.72 | – | +5.39 | +15.43 | +17.84 | +10.27 |
| 10×10cm$^2$ (15MV) | MC | +0.49 | −0.7 | −0.74 | −0.12 | +1.43 | −1.84 | +0.07 | −1.44 |
| | MB | −0.26 | +0.29 | +1.42 | +2.16 | +2.82 | +0.83 | +2.46 | +3 |
| | ETAR | +0.26 | +3.04 | +5.13 | +3.78 | +3.37 | +2.6 | +5.6 | +3.49 |
| 4×4cm$^2$ (15MV) | MC | −0.11 | −0.29 | −1.96 | – | +0.02 | +1.14 | −0.67 | +1.2 |
| | MB | +8.06 | +24.1 | +25.85 | – | +7.82 | +23.38 | +26.03 | +9.15 |
| | ETAR | +8.5 | +27.44 | +29.94 | – | +8.13 | +26.24 | +29.42 | +9.79 |

When the beam enters lung tissue there is less attenuation of primary photons and the absorbed dose to the lung increases. At the same time, the number of scattered photons generated in the lung is lower in comparison to unit density media and this causes some reduction in lung dose. For a 10×10cm$^2$ field the former effect dominates so that overall the absorbed dose to lung tissue increases. As expected, doses in the lung regions of the thorax phantom are higher than at the same depths in the homogeneous water phantom.

For 4×4cm$^2$ field size absorbed dose in the lung drops rapidly beyond unit density/lung density interface for both energies. This is in contrast to the situation for the 10×10cm$^2$ fields. It has been reported by several investigators that lateral electronic equilibrium does not exist in lung tissue for small field irradiations using high energy photons [19–21,27–30]. This causes significant reduction in the dose to the lung and becomes more pronounced at smaller field sizes and higher energies. Our results are in complete accordance with results of previous studies [19–21]. Although more primary photons reach the lung due to less attenuation of lung tissue, the lateral electronic disequilibrium causes a severe reduction in dose. The MB and ETAR methods overestimate lung doses and also in unit density media at points immediately downstream of the low density regions, such as in the mediastinum and distal chest wall.

Maximum local differences between calculation and measurement are +32.6% and +28.4%, for MB and ETAR respectively. These occur for 15MV posterior irradiations due to the greater thickness

of lung tissue traversed by the beam in the posterior direction. In a similar study, a maximum difference of 39% between ETAR and measurement was seen inside lung equivalent material in a 2×2cm$^2$ 18MV x-ray beam [30].

For the MC method, all measurement points agreed with calculation to within ±2% of local dose, with there being no observed dependency on energy and field size. This level of agreement is thought to be within the error due to the 1mm experimental uncertainty in positioning the ionization chamber.

Although MB and ETAR methods are not accurate for small field irradiations in the lung, they show better performance for points in the mediastinum and distal chest wall pending existence of lateral electronic equilibrium.

The energy deposited at a point is due to secondary electrons. The assumption used by both MB and ETAR methods that the dose at a given point is proportional to the x-ray fluence at that point may be acceptable for $^{60}$Co photons, but not for 8 and 15MV photons where the range of secondary electrons is up to several centimetres. For example, for a 15MV beam this range in lung with density of 0.33g/cm$^3$ can reach up to 9cm in the forward direction and for electrons that scatter laterally it can be as long as 5cm [12].

For 4×4cm$^2$ field size, there are secondary build-up regions in both cases and energies. This happens when the beam enters from the lung into the chest wall or mediastinum. The extent of secondary build-up region increases with energies for our cases. The presence of secondary build-up regions beyond the lung/unit density interfaces is predicted accurately by the MC method, whereas the lack of secondary electron transport in MB and ETAR makes them insensitive to these.

In the research of Saitoh et al, dose distribution of narrow beams of 6 and 10MV photons for small lung tumour was studied using the Monte Carlo method [20]. For 4×4cm$^2$ field size, they showed that there are build-up and build-down regions at the interface of chest wall and lung and the relative dose in the lung was lower than in the homogeneous case; the underdosage of lung increased with energy due to increased range of recoil electron in lung tissue. For small field irradiations in the lung, there is an electronic disequilibrium region after the chest wall and lung interface and the extent of this region increases with photon energy. It is impossible to calculate the dose in this area with conventional treatment planning systems (TPSs) [29,30]. However, Monte Carlo and Convolution/Superposition methods have shown better accuracy in this case [19,30]. In a recent study of Arnfield et al. on the accuracy of lung dose calculations by Collapsed Cone Convolution (CCC), Batho, and Monte Carlo methods, they showed that the CCC and MC methods perform better and are sensitive to absorbed dose changes due to electronic disequilibrium at interfaces and lateral electronic disequilibrium in the lung for small fields. However, there was up to 5% error for the CCC method for points beyond the lung [19].

Recently, Plessis et al. compared Batho and ETAR methods on the Cadplan treatment planning system for CT-based patient models [18]. They showed that these methods overestimate absorbed doses in the lung for small field sizes. Also they showed that these methods perform similarly (within 2%) in the lung. In our study similar results are seen and both algorithms perform within 3% in the lung. However, they did not perform a quantitative study and their study lacked validations by experimental measurements.

It is found from our results that both MB and ETAR methods implemented on the Eclipse treatment planning system for 3D-conformal treatment are not accurate enough for small lung dose calculations. This deficiency of Eclipse TPS may significantly compromise the advantages of 3D conformal treatments in the thorax region by underdosage of target volume in the lung and points beyond the low-density region such as the mediastinum and distal chest wall. Consequently, dose calculation errors could have a great effect on tumour control, and the advantages of new treatment modalities such as 3D-conformal radiotherapy and IMRT in the thorax region could be diminished or even undermined due to dose calculation inaccuracies.

## Conclusions

In this research we compared two analytical inhomogeneity correction methods, Modified Batho and Equivalent TAR, implemented on the Eclipse treatment planning system with the Monte Carlo method and ionization chamber measurements for thorax fields. Our MC simulations showed dose build-up and build-down regions at lung/unit density interfaces, but both analytical methods were unable to predict interface doses. This problem originates from the fact that these

methods are not able to model secondary electron transport in irradiated media. Other TPSs employing conventional algorithms are expected to perform in a similar manner. Our study findings showed great differences between both analytical methods and measurements for 4×4cm$^2$ field sizes for points in the lung. However, the results of these methods for 10×10cm$^2$ field size were comparable with measurements and MC results. Our study recommends using the MC method for small-field lung dose calculations.

## REFERENCES:


1. Brahme A, Chavaudra J, Landberg T et al: Accuracy requirements and quality assurance of external beam therapy with photons and electrons. Acta Oncol, 1988; 27(Suppl.1): 1–26
2. Thwaites DI: Uncertainties at the end point of the basic dosimetry chain. In: measurement assurance in dosimetry, IAEA, Vienna, 1994
3. Batho HF: Lung correction in cobalt-60 beam therapy. J Can Assoc Radiol, 1964; Xv: 79–83
4. Young ME, Gaylord JD: Experimental tests of corrections for tissue inhomogenities in radiotherapy. BJR, 1970; 43: 349–55
5. Mesbahi A, Allahverdi M, Gheraati H, Mohammadi E: Experimental evaluation of ALFARD treatment planning system for 6MV photon irradiation: A lung case study. Rep Pract Oncol Radiother, 2004; 9(6): 217–21
6. El-Khatib E, Battista JJ: Accuracy of lung dose calculations for large fields irradiation with 6MV X-rays. Med Phys, 1986; 13(1): 111–5
7. Kornelson RD, Young ME: Changes in the dose-profile of a 10MV X-ray beam within and beyond low density material. Med Phys, 1982; 9: 114–6
8. Van Dyk J, Battista JJ, Rider WD: Half-body radiotherapy: the use of computed tomography to determine the dose to the lung. Int J Rad Oncol Biol Phys, 1980; 6: 436–70
9. Lulu BA, Bjarngard BE: Batho correction factor with scatter summation. Med Phys, 1982; 9(3): 372–7
10. Young ME, Kornelson RO: Dose corrections for low density tissue inhomogenities and air channels for 10MV X-rays. Med Phys, 1983; 10: 450–5
11. Orthon CG, Mondalek PM, Spicka JT et al: Lung corrections in photon beam treatment planning: are we ready? Int J Rad Oncol Biol Phys, 1984; 10: 2191–9
12. Mackie TR, El-Khatib E, Battista JJ et al: Lung dose corrections for 6 and 15M X-rays. Med Phys, 1985; 12(3): 327–32
13. El-Khatib E, Evans M, Pla M, Cunningham JR: Evaluation of lung dose correction methods for photon irradiations of thorax phantoms. Int J Radiat Oncol Biol Phy, 1989; 17: 871–8
14. Demarco JJ, Solberg TD: A CT-based Monte Carlo tool for dosimetry planning and analysis. Med Phys, 1998; 25(1): 1–11
15. Solberg TD, DeMarco JJ, Chetty IJ et al: A review of radiation dosimetry application using the MCNP Monte Carlo code. Radiochim Acta, 2001; 89: 337–55
16. Martens C, Reynaert N, De Wagter C et al: Undedosage of the upper-airway mucosa for small fields as used in intensity-modulated radiation therapy: A comparison between radiochromic film measurements, Monte Carlo simulations, and collapsed cone convolution calculations. Med Phys, 2002; 29(7): 1528–35
17. Ma CM, Pawlicki T, Jiang SB et al: Monte Carlo verification of IMRT dose distributions from a commercial treatment planning optimization system. Phys Med Biol, 2000; 45: 2483–95
18. Plessis FCP, Willemse CA, Lotter MG: Comparison of the Batho, ETAR and Monte Carlo dose calculation methods in CT based patient models. Med Phys, 2001; 28(4): 582–9
19. Arnifield MR, Siantar CH, Cox L, Mohan R: The impact of electron transport on the accuracy of computed dose. Med Phys, 2000; 27(6): 1266–74
20. Saitoh H, Fujisaki T, Sakai R, Kunieda E: Dose distribution of narrow beam irradiation for small lung tumor. Int J Radiat Oncol Biol Phys, 2002; 53(5): 1380–7
21. Chetty IJ, Charland PM, Tyagi N, Mc Shan D: Photon beam relative dose validation of DPM Monte Carlo code in lung-equivalent media. Med Phys, 2003; 30(4): 563–73
22. Laub WU, Bakai A, Nüsslin F: Intensity modulated irradiation of a thorax phantom: comparisons between measurements, Monte Carlo calculations and pencil beam calculations. Phys Med Biol, 2001; 46(6) 1695–706
23. Sheikh-Bagheri D, Rogers DWO: Sensitivity of megavoltage photon beam Monte Carlo simulations to electron beam and other parameters. Med Phys, 2002; 29(3): 379–90
24. Tzedakis A, Damilakis JE, Mazonakis M et al: Influence of initial electron beam parameters on Monte Carlo calculated absorbed dose distributions for radiotherapy photon beams. Med Phys, 2004; 31(4): 907–13
25. Mesbahi, A, Fix M, Allahverdi M et al: Monte Carlo calculation of Varian 2300C/D Linac photon beam characteristics: a comparison between MCNP4C,GEANT3 and measurements. Appl Radiat Isotop, 2005; 62: 469–77
26. Venselaar J, Welleweerd H, Mijnheer B: Tolerances for the accuracy of photon beam dose calculations of treatment planning systems. Radiother Oncol, 2001; 60: 191–201

27. White PJ, Zwicker RD, Huang DT: Comparison of dose homogeneity effects due to electron equilibrium loss in lung for 6MV and 15MV photons. Int J Radiat Oncol Biol Phys, 1996; 34: 1141–6

28. Yorke E, Harisiadis L, Wessels B et al: Dosimetric considerations in radiation therapy of coin lesions of the lung. Int Rad Oncol Biol Phys, 1996; 34: 481–7

29. Cranmer-Sargison G, Beckham WA, Popescu IA. Modelling an extreme water-lung interface using a single pencil beam algorithm and Monte Carlo method. Phys Med Biol, 2004; 49: 1557–67

30. Carrasco P, Jornet N, Dutch MA et al: Comparison of dose calculation algorithms in phantoms with lung equivalent heterogeneities under conditions of lateral electronic disequilibrium. Med Phys, 2004; 31(10): 2899–911